RESEARCH PAPER

Effect of viscosities of dispersed and continuous phases in microchannel oil-in-water emulsification

Koen van Dijke · Isao Kobayashi · Karin Schroën · Kunihiko Uemura · Mitsutoshi Nakajima · Remko Boom

Abstract Although many aspects of microchannel emulsification have been covered in literature, one major uncharted area is the effect of viscosity of both phases on droplet size in the stable droplet generation regime. It is expected that for droplet formation to take place, the inflow of the continuous phase should be sufficiently fast compared to the outflow of the liquid that is forming the droplet. The ratio of the viscosities was therefore varied by using a range of continuous and dispersed phases, both experimentally and computationally. At high viscosity ratio (η_d/η_c), the droplet size is constant; the inflow of the continuous phase is fast compared to the outflow of the dispersed phase. At lower ratios, the droplet diameter increases, until a viscosity ratio is reached at which droplet formation is no longer possible (the minimal ratio). This was confirmed and elucidated through CFD simulations. The limiting value is shown to be a function of the microchannel design, and this should be adapted to the viscosity of the two fluids that need to be emulsified.

Keywords Microchannels · Uniform droplets · Viscosity · CFD

K. van Dijke · K. Schroën (✉) · R. Boom
Food Process Engineering Group, Wageningen University,
P.O. Box 8129, 6700 EV Wageningen, The Netherlands
e-mail: karin.schroen@wur.nl

I. Kobayashi (✉) · K. Uemura · M. Nakajima
Food Engineering Division, National Food Research Institute,
Kannondai 2-1-12, Tsukuba, Ibaraki 305-8642, Japan
e-mail: isaok@affrc.go.jp

M. Nakajima
Graduate School of Life and Environmental Sciences, University
of Tsukuba, Tennoudai 1-1-1, Tsukuba, Ibaraki 305-8572, Japan

1 Introduction

Microfluidic emulsification of immiscible fluids is of interest to several different application areas because of the high monodispersity of the obtained emulsions. The gentle and controlled formation of droplets is a benefit compared to traditional techniques which use intense force fields to disrupt large, premixed droplets into smaller and relatively polydisperse droplets. Commonly used and studied microtechnological emulsification devices can be driven by transversal flow (T- and Y-junctions (Garstecki et al. 2006; van der Graaf et al. 2005; Steegmans et al. 2009)), coflow (flow-focusing devices (Anna et al. 2003; Xu and Nakajima 2004)) or by interfacial tension (also called spontaneous droplet formation; grooved microchannels (Kawakatsu et al. 1997) and straight-through microchannels (Kobayashi et al. 2002)). Several researchers explored the influence of system parameters on micro-emulsification processes and observed that droplet size can be varied by the design of the microfluidic device (Van Dijke et al. 2008; Sugiura et al. 2002; Kobayashi et al. 2005), the flow rates of both phases (Garstecki et al. 2004), and the properties of the liquids and other ingredients (Saito et al. 2005; Vladisavljević et al. 2008).

Spontaneous droplet formation devices yield a combination of good monodispersity, relatively high throughputs (if parallelized), and robustness. The influence of many of the geometric parameters in these systems has been explored. However, the effect of viscosity of both phases is not yet clear, and is therefore explored here. During the snap-off of a droplet, the dispersed phase flowing out of the nozzle has to be replaced by an equal amount of continuous phase; otherwise the drainage of the dispersed phase out of the nozzle will be hindered and the droplet will not snap off. In grooved microchannel devices, the terrace structure

facilitates the inflow of the continuous phase. Kobayashi et al. (2004) found a minimum aspect (length/width) ratio for straight-through channels of 3–3.5 necessary to produce oil droplets. At a lower aspect ratio, the droplet will block the complete opening of the terrace, preventing inflow of the continuous phase, and thus preventing snap-off of the droplet. This was confirmed by Rayner et al. (2004) using static minimization of the surface area during the process. Next to that, dynamic interfacial tension effects may occur, and if diffusion is the driving force behind surfactant transport to the interface, an effect of continuous phase viscosity is expected here too.

We here report on the effect of the viscosities of the phases by performing emulsification experiments with several dispersed phases into various polyethylene glycol (PEG)-water-SDS mixtures as continuous phase, and by performing fluid dynamics calculations of a comparable MC-system with a single channel to gain fundamental understanding of the observations.

2 Materials and methods

2.1 Chemicals

In the emulsification experiments, refined soybean oil, hexadecane, and several silicon oils (S200, S500, S1000, and S5000) were used as dispersed phase. Polyethylene glycol (PEG) was added in different amounts to MilliQ water with 1 wt% sodium dodecyl sulfate (SDS) to vary the viscosity (η_c) of the continuous phase. All chemicals were purchased from Wako Pure Chemical Industries, Ltd. (Osaka, Japan), except for the silicon oils which came from Shin-Etsu Chemical Co., Ltd. (Tokyo, Japan). The viscosities of the chemicals and mixtures were measured with a Vibro viscometer SV-10 (A&D Company, Ltd., Tokyo, Japan), except for the silicon oils of which the viscosities

were given by the manufacturer. The density (ρ) was determined with a density meter (model DA-130N, KEM Co., Ltd., Kyoto, Japan). The static equilibrium interfacial tensions (σ^{eq}) were measured with the pendant drop method (PD-W, Kyowa Interface Science Co., Ltd., Saitama, Japan). All measurements and experiments were performed at 25°C.

In Table 1, the viscosity, density, equilibrium interfacial tension of the dispersed phases in contact with SDS solution ($\sigma^{eq,SDS}$) and the average equilibrium interfacial tensions of the oil in contact with a PEG-SDS-solution ($\sigma^{eq,PEG}$) are shown. Next to that, the viscosity and density of the water phases are given.

The addition of PEG to the water-SDS solutions results in an increased viscosity of the continuous phase; up to 68.2 mPa s for a 20 wt% PEG—1wt% SDS-water solution. The equilibrium interfacial tension is influenced by the oil that is used, with the most apolar oils having the highest values. Further, addition of PEG plays a role as is reflected in SDS systematically giving lower values when in absence of PEG. The influence of the PEG concentration on the interfacial tension is however minor, and therefore these values are represented as the average of all the measurements done with different PEG concentrations for a specific oil.

2.2 Microchannel device and peripherals

In this study, we used a silicon 1.5×1.5 cm^2 grooved microchannel device with 150 channels at each side of the chip; for simplicity reasons we will call this chip design 1. In Fig. 1, schematic representations of the hydrophilic MC array plate with several relevant dimensions of chip design 1 are shown. The channel depth (H) is 8 μm, the channel length (L_c) is 25.3 μm, and terrace length (L_T) is 51.7 μm. The cross-section of the channel is shown in Fig. 1b. The hydraulic diameter (d_{eq}), which is defined as four times the

Table 1 Measured properties of phases used in the experiments at 25°C

	Dispersed phase				PEG in water (wt%)[b]	Continuous phase	
	η_d (mPa s)	ρ_d (kg m^{-3})	$\sigma^{eq,SDS}$ (mN m^{-1})	$\sigma^{eq,PEG}$ [a] (mN m^{-1})		η_c (mPa s)	ρ_c (kg m^{-3})
Hexadecane	2.32	769	9.1	10.7	0	0.91	997
Soybean oil	48.7	916	4.7	8.1	1	1.40	1000
Silicon oil	200	965	9.7	12.5	2.5	2.10	1002
	500	970	10	–	5	4.83	1006
	1000	970	10.6	13.3	7.5	7.84	1011
	5000	970	15	–	10	13.9	1015
					20	68.2	1032

[a] Average value is average for all PEG concentrations; $\sigma^{eq,PEG}$ decreased only slightly at higher wt% PEG, therefore, only one value is shown to represent all in the series

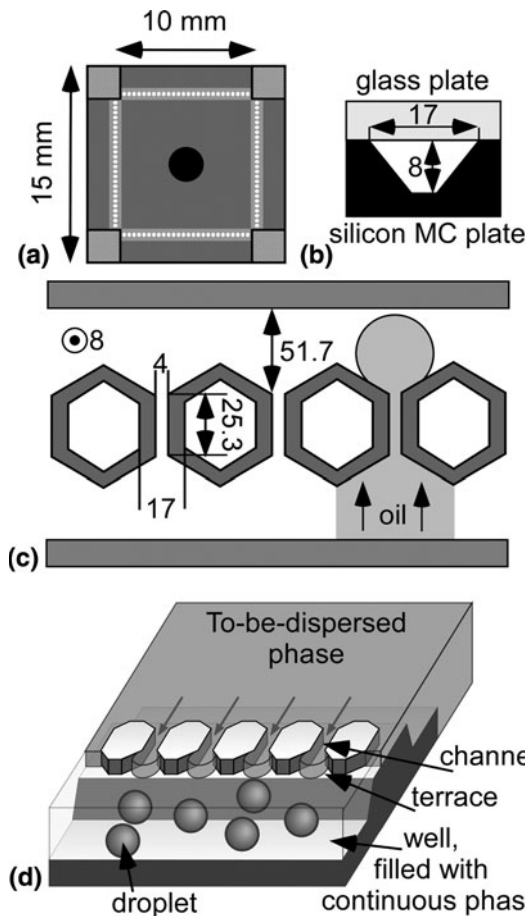[b] All solutions contain 1 wt% SDS

Fig. 1 Schematic representation of the microchannel system. **a** chip layout, **b** cross-section of a microchannel, **c** top-view of three microchannels, **d** three-dimensional drawing of part of microchannel system producing droplets. Dimensions are in micrometers if not mentioned

area over the perimeter, is 8 μm. Before the first experiments were carried out, the chip was subjected to plasma oxidation in a plasma reactor (PR41, Yamato Science Co. Ltd., Tokyo, Japan). After each measurement, the chip was cleaned with ethanol and a neutral detergent solution (Clean Ace Neutral) in an ultrasound water bath for 20 min and stored in 0.1 M nitric acid for future usage. We also used a comparable microchannel chip albeit with a longer channel ($L_{c,MCL} = 70$ μm), shorter terrace ($L_{T,MCL} = 30$ μm), and channel depth ($H_{MCL} = 7$ μm) in a few measurements; and this chip we will indicate with design 2. The MC plates were placed in the module shown in Fig. 2, which was initially filled with the continuous phase; we observed droplet formation with a microscopic high-speed video system.

The to-be-dispersed phase was pressurized via hydrostatic pressure (by increasing the height of the supplying vessel) until the break-through pressure was reached and droplets start to form. (Fig. 1d shows a schematic
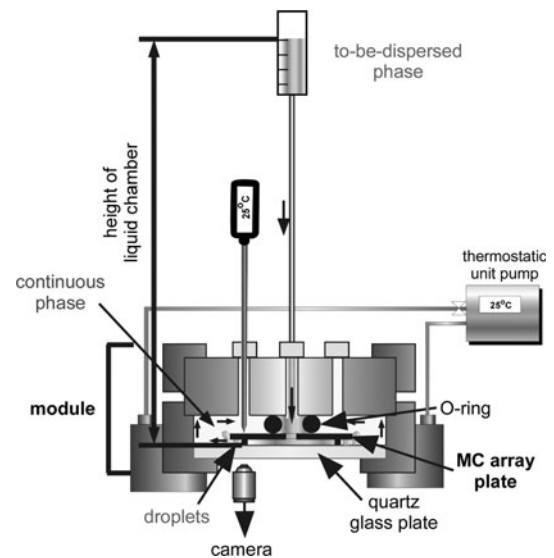

Fig. 2 Schematic drawing of all peripherals for microchannel emulsification

representation of four active microchannels.) The theoretical break-through pressure for a cylindrical channel with diameter D_{ch} and contact angle θ, can be calculated with Laplace's law:

$$\Delta P_{min} = \frac{4\sigma \cos \theta}{D_{ch}} \tag{1}$$

This equation can be used to calculate the approximate value of the break-through pressures in the systems used in this work.

2.3 Analysis

The number-averaged diameters of around 100 produced droplets were measured using image analysis software (WinRoof, Mitani Co., Ltd., Fukui, Japan). Characteristic droplet formation times were also determined by the same software, one droplet formation cycle is depicted in Fig. 3; droplets in the well could easily be recorded and analyzed, see also Fig. 4.

2.4 Simulations

To simulate a droplet formation cycle in a single microchannel, the fully three-dimensional Volume-of-Fluid method incorporated in CD-Adapco's Star-CD (version 4.0) was used. Details and validation of the method in this context are both described in Van Dijke et al. (2008). The grid was as close as possible the system used in this study, albeit that for simplicity reasons, we defined a rectangular terrace with $L_T = 50$ μm and a terrace width (W_T) of 98 μm. The square-shaped supply channel was defined having a width $W_c = 8$ μm and $L_c = 25$ μm. Both channel
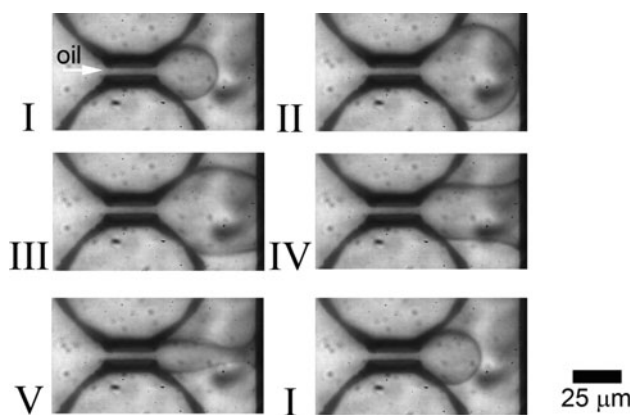
Fig. 3 A droplet formation cycle; the oil is pushed into the microchannel from the left side of the image onto the terrace, where it forms a disk which eventually reaches the end of the terrace and snaps off to form a droplet

and terrace are 8 μm in depth and a symmetry plane was applied in the middle. We used a static inlet pressure-boundary on the channel entrance, and a reference outlet pressure-boundary of 0 Pa. The contact angle (θ) was set at 10° to represent a realistic hydrophilic surface. Surfactant dynamics cannot be taken into account (as is currently the case in any other computation package); we assumed no cross-flow of the continuous phase. At $t = 0$, the oil–water interface is flat at position $x = 23$ μm, just before the channel ends on the terrace. The material properties were defined as measured for the systems with 1% SDS solution, except for the viscosity values. Contrary to the experiments, in the computations we could change the viscosity of the continuous phases without affecting the interfacial tension or density (in reality changes are caused by adding PEG as denoted in Table 1). As a result, we were able to define the applied pressure at a value just above the

minimally required pressure for all systems, which allowed us to consider viscosity effects only.

The average computation time was about 5 days when the grid domain was divided over two nodes running under Linux 2.6.8.; each with two 2994 MHz Intel Pentium IV XEON processors and a physical memory of 3044 MB. Due to computation capacity limitations, only hexadecane was used in the simulations as dispersed phase. The pressure values at different positions and time stages during droplet formation were extracted with Pro-Star, the post-processing program of the software package and enhanced and combined with Canvas software (version 11, ACD Systems of America, Inc.); see Fig. 6.

3 Results and discussion

3.1 Emulsification

Figure 4 shows three microscopic photographs of droplet formation in a grooved microchannel system just above break-through pressure where uniform droplets can be produced (a–c), and a picture of a system in the blow-up regime (d). Although the pictures seem crowded, it is in case (a–c) possible to determine the size of the droplets.

In (a), hexadecane droplets are formed in a continuous phase with viscosity $\eta_c = 4.83$ mPa s (giving a viscosity ratio of 0.48, see Eq. 2). The low viscosity of hexadecane results in a high rate of droplet formation. The droplets are non-spherical in front of the channel outlet: the viscous continuous phase hinders the motion of the droplets, and squeezes them together. Further away from the terrace, the droplets become more spherical. In a continuous phase with low viscosity, the droplets were spherical everywhere. Figure 4b shows droplet formation of a silicon oil with

Fig. 4 Typical emulsification results. **a** Squeezed-hexadecane droplets in 5 wt% PEG—1 wt% SDS solution, **b** Silicon oil ($\eta_d = 1000$ mPa s) in 20 wt% PEG—1 wt% SDS solution, **c** Silicon oil ($\eta_d = 5000$ mPa s) in 1 wt% SDS solution, **d** blow-up at elevated pressure, shown at lower magnification
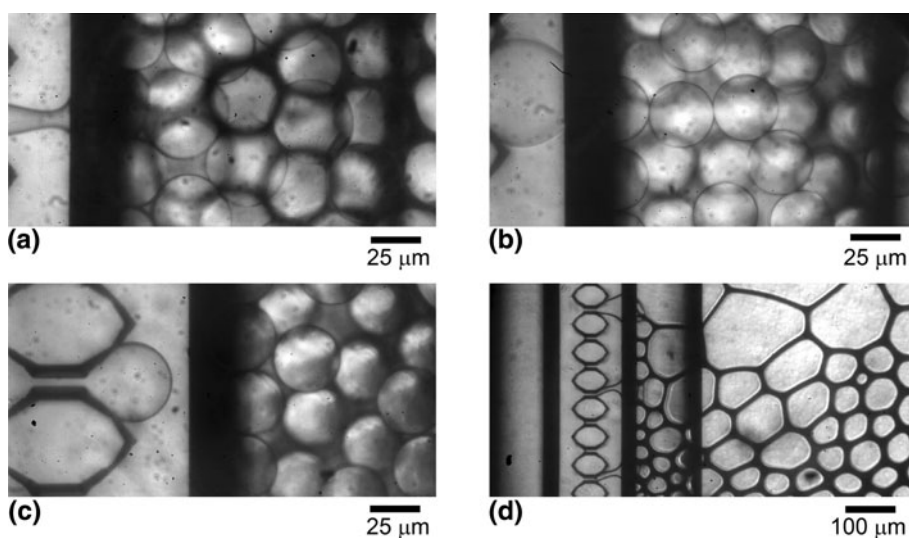
Table 2 Results of performed experiments with chip design 1

Oil	η_c (mPa s)	D_{drop} (µm)	c.v. (%)	t_{drop} (ms)	Oil	η_c (mPa s)	D_{drop} (µm)	c.v. (%)	t_{drop} (ms)
Hexadecane, $\eta = 2.32$ mPa s	0.91	34.8	2.5	42	Silicon oil, $\eta = 200$ mPa s	0.91	32.6	2	169
	1.40	36.8	3.7	30		4.83	34.6	4.1	303
	2.10	39.8	3.9	33		13.9	34.4	5.1	347
	4.83	41.6	9.6	34		68.2	36.2	9.3	470[c]
	7.84	–			Silicon oil, $\eta = 500$ mPa s	0.91	33.0	4.2	284
	13.9	–			Silicon oil, $\eta = 1000$ mPa s	0.91	33.6	2.7	442
	68.2	–				4.83	33.6	3.3	1236
Soybean oil, $\eta = 48.7$ mPa s	0.91	32.0	2.1	404		13.9	33.6	4.1	1284
	4.83	33.4	3.8	290		68.2	33.6	3.7	1714
	13.9	34.4	2.9	518	Silicon oil, $\eta = 5000$ mPa s	0.91	33.6	3.8	2420
	68.2	39.6	12.2	432[c]					

[c] Time dependent blow-up

viscosity $\eta_d = 1000$ mPa s in a 20 wt% PEG—1 wt% SDS aqueous solution with $\eta_c = 68.2$ mPa s (viscosity ratio = 14.7). Although the continuous phase is more viscous than in (a), the formed droplets are spherical and that are most probably due to the much slower droplet formation, which will be discussed later in more detail. In (c), oil with an even higher viscosity is used, in a 1 wt% SDS solution, and again spherical droplets were formed. Most emulsification experiments performed at pressures below the blow-up pressure resulted in equally sized droplets with a coefficient of variation below 5% (see also Table 2). In highly viscous continuous phases, the c.v. of droplets formed from low viscosity oils is somewhat higher, and this is probably caused by the deformed droplets, which are slightly more difficult to characterize. In picture (d), blow-up of a soybean oil system in a continuous phase with $\eta_c = 68.2$ is shown (viscosity ratio 0.71). This occurs at elevated pressures, which is similar to earlier reported behavior of MC systems. In contrast to systems with lower viscosity of the continuous phase, this blow-up behavior is self re-enforcing: as soon as one channel starts to blow-up all active channels will follow shortly thereafter. Besides, for some systems with high continuous phase viscosity, we observed time dependent blow-up, which implies that after several hundred droplets blow-up occurred without increasing the pressure. Most probably, this is caused by limitation of surfactant transfer to the interfaces which will be discussed later. Table 2 shows an overview of the droplet diameters, corresponding coefficients of variation, and total droplet formation times of the experiments performed with microchannel design 1.

To compare the experiments, we have chosen to define the viscosity ratio (ξ) as the ratio of the to-be-dispersed phase viscosity (η_d) over the continuous phase viscosity (η_c):

$$\xi = \frac{\eta_d}{\eta_c} \qquad (2)$$

and the dimensionless droplet diameter D as the resulting droplet diameter D_{drop} divided by the height of the terrace H:

$$D = \frac{D_{drop}}{H} \qquad (3)$$

The effect of the viscosity ratio on the dimensionless droplet diameter is shown in Fig. 5.

In spite of the big variation in actual viscosity values of the to-be-dispersed and continuous phases, all data collapse
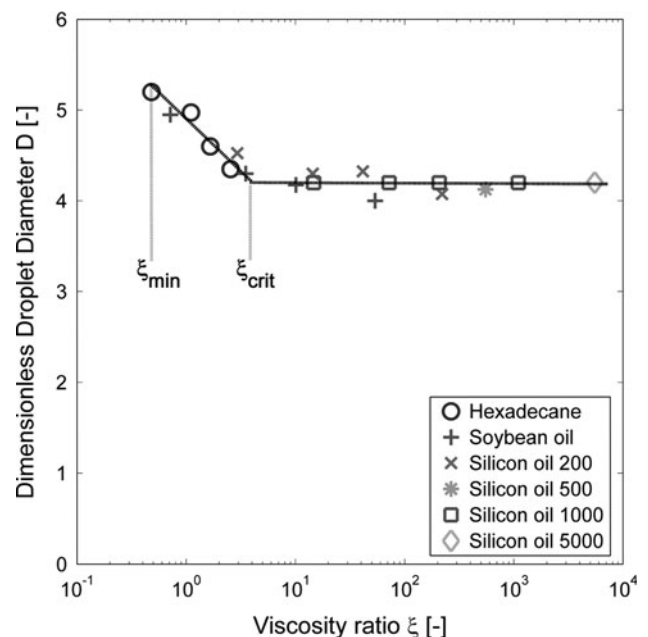

Fig. 5 Dimensionless droplet diameter in the stable droplet formation regime as a function of the viscosity ratio for chip design 1

onto a dimensionless master curve. If the viscosity ratio is above a certain value (ξ_{crit}), the droplet size is not influenced by the viscosity ratio. The droplet diameter is only affected at low viscosity ratio, below ξ_{crit}, where the droplet size increases with decreasing viscosity ratio. Below a minimal value of the viscosity ratio, $\xi_{min} = 0.48$, we were not able to form droplets with microchannel design 1. We will now discuss the observed results, also in relation to simulation results, taking two phenomena as a starting point: continuous phase inflow and dynamic interfacial tension.

3.2 Continuous phase inflow

For microchannel systems, it is known from literature that they facilitate inflow of the continuous phase near the location of droplet snap-off. In grooved microchannels, as well as in asymmetric straight-through channels, the terrace structure enhances microchannel emulsification (Sugiura et al. 2002; Kobayashi et al. 2004; Kobayashi et al. 2005) and for oblong straight-through channels it is well documented that the aspect ratio of the channels needs to be larger than 3–3.5 in order to obtain monodisperse droplet formation. Through CFD simulations, it was shown that this minimal aspect ratio was indeed necessary to have enough intrusion possibilities for the continuous phase; i.e.,

water (Kobayashi et al. 2004). At a lower aspect ratio, the growing droplet will completely block the microchannel, and inhibit the ingression of the continuous phase. This is however a static effect.

In this work, we take the CFD simulations a step further and use higher continuous phase viscosities to understand the observed dynamics in the experiments. As an example, we show in Fig. 6, the pressure fields at similar stages in droplet formation plotted for a continuous phase viscosity of $\eta_c = 0.91$ mPa s ($\xi = 2.55$) and $\eta_c = 4.83$ mPa s ($\xi = 0.48$); both simulations are for hexadecane as to-be-dispersed phase, and other details are given in the Sect. 2.

In Fig. 6, only half of the terrace structure is shown to allow detailed observation of the pressure field; a symmetry plane is used in the middle. As the computational grids are slightly rotated, the top views as well as the cross-sections are visible. The pressure values relative to atmospheric pressure are indicated in the 'color' bars (the one with the full color is for the negative range, the one with the hatched lines is for the positive relative pressures); the interface is at the black line. Due to the Laplace pressure over the interface between water and oil, the pressure values in the to-be-dispersed phase are much higher and gradients are larger compared to the continuous phase.

In Fig. 6, stage I is the inflation stage where the oil flows onto the terrace in a disk-like shape. Similar behavior is

Fig. 6 Pressure fields during three stages of droplet formation for emulsification systems with a high (*left*) and low viscosity ratio (*right*)
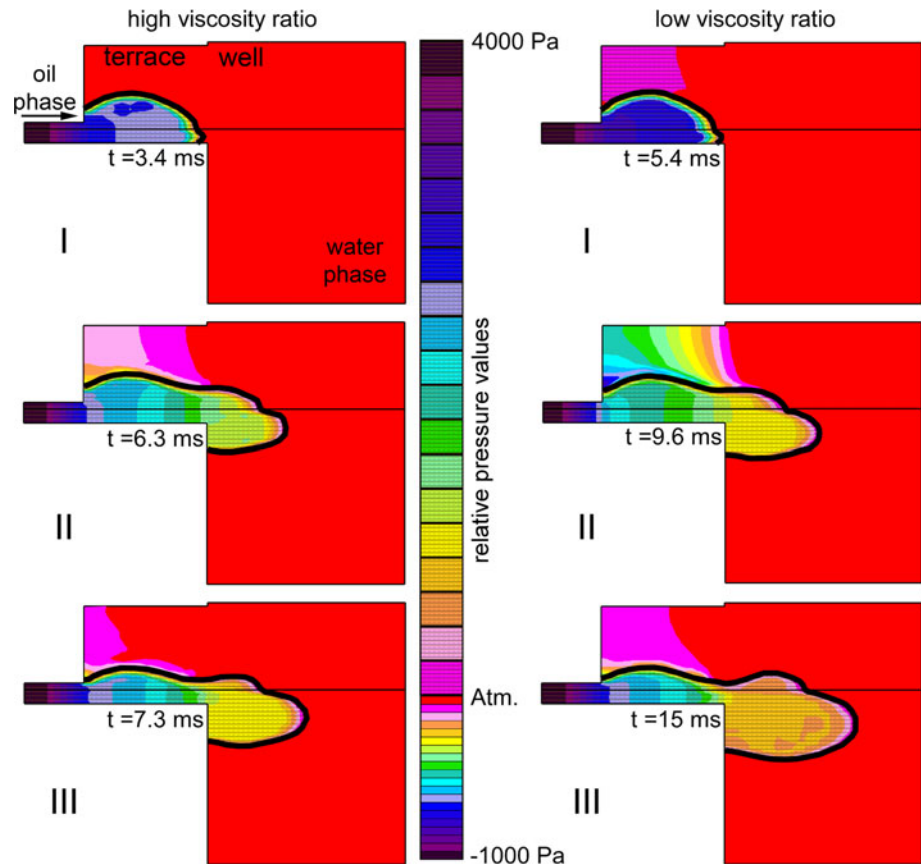
observed in both situations, although at low ξ the process is somewhat slower. The crucial difference between high and low continuous phase viscosity ratios becomes visible during stage II, where the disk-like oil shape on the terrace flows into the spherical growing droplet in the well. While the terrace is emptied, the generated inward gradient on the terrace causes the continuous phase to flow onto it. With a higher viscosity of the continuous phase, this gradient is clearly steeper, resulting in lower values of the pressure. In stage III, the droplet is close to snap-off, and the gradients that were present in the continuous phase during stage II, have practically leveled out again.

The analytical model derived for MC systems in Van Dijke et al. (2008), was developed for the situation with a high ξ (low viscosity of the continuous phase). Given the differences in local pressures that we noted in the simulation, the analytical model should be refined, since it is based on the local pressures at three locations in the system. For the model, we use the break-through pressure mentioned earlier (Eq. 1), which is the lowest pressure applied at the channel entrance which enables the oil to flow into the channel, the pressure in the oil on the terrace (P_d), and the pressure in the droplet (P_{drop}). Break-up occurs if the flux to the droplet (Φ_n: caused by a pressure difference between terrace and droplet) exceeds the supplying flux through the channel (Φ_{ch}: caused by a pressure difference between channel entrance and terrace), so:

$$\Phi_n > \Phi_{ch} \tag{4}$$

If this criterion is fulfilled immediately after emptying the terrace, the process generates small droplets and is in the monodisperse droplet generation regime. If not, a quasi-static neck will be present to supply oil to the droplet until the criterion is fulfilled.

The pressure in the droplet ΔP_{drop}, defined by:

$$\Delta P_{drop} = \frac{2\sigma}{R_d} \tag{5}$$

(with, σ the interfacial tension, and R_d the droplet diameter), and the break-through pressure at the channel entrance (Eq. 1) will not be affected by the continuous phase viscosity. In contrast, as shown in the simulations, a higher continuous phase viscosity results in a steeper gradient and lower pressure values in the continuous phase on the terrace (P_c) as can be seen in Fig. 6, and this effectively influences the pressure differences in the to-be-dispersed phase (P_d) on the terrace, which follow from:

$$\Delta P_{terrace} = P_d - P_c = \sigma \left(\frac{1}{R_1} + \frac{1}{R_2} \right) \cos\theta \tag{6}$$

in which, R_1 and R_2 are the principle radii of curvature of the oil shape on the terrace, and θ is the contact angle. R_1 is determined by the height of the terrace, H, while R_2 varies

during stage II in Fig. 6 (emptying terrace), and further, the contact angle is assumed to be constant. In case of a higher viscosity of the continuous phase, the pressure in the oil phase on the terrace (P_d) is lower, and consequently, the supply flow of dispersed phase from the channel to the terrace will be high. As a result, a larger volume of dispersed phase will flow into the well during this stage of droplet formation, and larger droplets will be formed at low ξ, as is visible in stage II of the droplet formation process in Fig. 6.

3.3 Interfacial tension

From the results depicted in Fig. 5 and Table 2, and the measured static equilibrium interfacial tensions shown in Table 1, we can conclude that there is no direct link between static interfacial tension and resulting droplet size. There seems to be a link between the static interfacial tension and the droplet formation times, as can be seen in Table 2. These observations are in line with the results from Sugiura et al. (2004), who also reported an influence on the time of droplet formation. The reason for more rapid droplet formation at higher interfacial tension values is the larger absolute pressure difference between the local pressures defined in the previous paragraph (the curvatures are expected to be similar); which is co-determined by the local interfacial tension.

If the process is extremely slow in every sense, the surfactant will have sufficient time to cover the surface area, and the interfacial tension will be equal to the equilibrium interfacial tension. However, given the timescales at which emulsification occurs, it is reasonable that in at least some of the experiments, dynamic interfacial tension effects play a role. Here we try to evaluate the importance of the dynamic interfacial tension by investigating the timescale for diffusion of the surfactant molecules (τ_d) for molecular diffusion near the droplets in laminar flow at low Reynolds numbers (Lucassen-Reynders and Kuijpers 1992):

$$\tau_d = \frac{2}{D_{diff}} \left(\frac{d\Gamma}{dc} \right)^2 \tag{7}$$

in which, D_{diff} is the diffusion coefficient of the surfactants, Γ the adsorbed amount and c the surfactant concentration. Further, the relative rate of new surface area creation (κ) can be defined as:

$$\kappa = \frac{d\ln A}{dt} \tag{8}$$

The numerical value of τ_d depends strongly on the concentration of the emulsifier, and its diffusion coefficient; theoretical values for SDS are in the order of 10^{-3} s (Vlahovska et al. 1997; Sasaki et al. 1977). The interfacial tension will be at its equilibrium value if the

diffusion of the surfactant molecules is fast enough to cover the newly created interface instantaneously:

$$\kappa = \frac{d \ln A}{dt} \ll (\tau_d)^{-1} \Rightarrow \sigma \approx \sigma^{eq} \qquad (9)$$

The interface will be free of emulsifier if:

$$\kappa = \frac{d \ln A}{dt} \gg (\tau_d)^{-1} \Rightarrow \sigma \approx \sigma^0 \qquad (10)$$

From the definition of the time scale of diffusion, it follows that τ_d is inversely proportional with the diffusion coefficient D_{diff}, and we expect D_{diff} inversely proportional to the viscosity, if we follow the Stokes–Einstein relation:

$$D_{diff} = \frac{k_B T}{6\pi \eta r} \qquad (11)$$

and this would imply that τ_d is proportional to the viscosity:

$$\tau_d \propto \eta_c \qquad (12)$$

We can approximate the surface creation rate from the droplet surface area A_{drop}, and the initial oil disk area A_{start} and the droplet formation cycle time t_{drop}:

$$\kappa \approx \frac{\ln A_{drop} - \ln A_{start}}{t_{drop}} \qquad (13)$$

Hexadecane has the fastest area creation rate in the performed experiments; κ ranges from 60 to 80 s^{-1}. Using the value of τ_d from literature, it can be concluded that for this low viscous continuous phase, diffusion is fast enough to cover the interface, $\kappa \ll (\tau_d)^{-1}$, and reduce interfacial tension instantaneously to a value close to its equilibrium value.

Increasing the viscosity of the continuous phase has two straightforward effects related to interfacial tension effects; it will lower the diffusional mobility of the surfactant (Eq. 12) and it will affect the droplet formation rate (see also Fig. 6), and thus the surface creation rate (κ). In addition, several indirect effects can influence droplet formation. An increase in dynamic interfacial tension value will influence the droplet formation rate as described earlier for a static value, therewith affecting its own dynamic behavior. The generation of a great multitude of droplets or smaller-sized droplets (total surface area formation larger) will result in a faster depletion of surfactant from the continuous phase, therewith inducing effects on droplet formation rate and stability. Further, we noted in our experiments that a very low cross-flow may need to be applied to supply 'fresh' surfactant (and transport of formed droplets that may hinder the surfactant supply process) especially at a high viscosity of the continuous phase, where blow-up is more likely to occur. Clearly, the cross flow does not initiate droplet formation, as would be the case in shear-driven systems.

In our CFD simulations, in which a constant interfacial tension was assumed, we see similar trends in droplet size as we found experimentally. For these low viscosity ratios, the influence of the dynamic nature of the interfacial tension on the droplet size in the monodisperse regime seems limited, and we expect that the differences in droplet size are caused by slower continuous phase inflow.

3.4 System design

Several aspects of droplet formation can be influenced with the design of the microchannel device, as is reported in various sources. When we summarize all these aspects, in combination with the explanation of the observed phenomena in this paper, we conclude that it should be possible to shift the droplet diameter versus viscosity ratio curve. For this, the system could be chosen such that it is beneficial for droplet formation at lower viscosity ratios, and this is expected to be the case for microchannels with shorter terraces where the inflow distance is correspondingly shorter. Therefore, we investigated a comparable MC system to prove that the design can indeed be used to improve the window of operation. In Fig. 7, the dimensionless diameters of droplets obtained with a system with a shorter terrace (and longer channel) (design 2) are added to the data presented earlier.

Because of the smaller terrace, smaller droplets can be formed, however more importantly, with this design, we were able to form equally sized droplets until a minimum value of $\xi_{min} = 0.16$. A shorter terrace length will result in
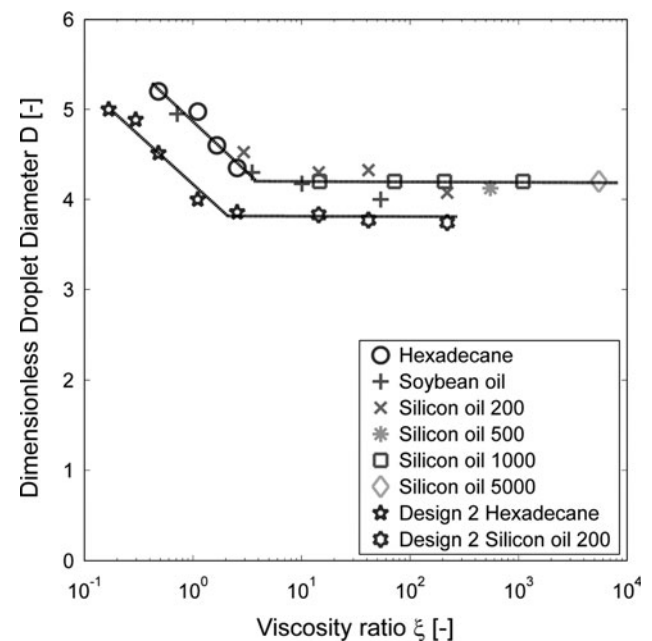

Fig. 7 Dimensionless droplet diameter as a function of the viscosity ratio; effect of channel design

a shorter inflow distance for the continuous phase which will be beneficial at low ξ as was expected. However, another aspect that is relevant is the length of the channels, and from literature (Sugiura et al. 2002; Van Dijke et al. 2008) it is known that longer channels result in more stable droplet generation. This study adds to this finding that long channels could also be beneficial for droplet formation at low viscosity ratios. A longer channel means a higher hydrodynamic flow resistance, which slows down the flow from channel to the terrace during droplet formation, therewith keeping the inflow of dispersed phase through the microchannel more constant, and through this also the entire droplet formation process. Clearly, both the terrace and channel length have a positive influence on microchannel emulsification.

In summary, from all our findings it is clear that not only the design of the microchannel itself is essential for stable emulsification, but that also the design needs to be adapted to the components (dispersed and continuous phases and surfactant) that are to be emulsified.

4 Conclusions

We report the effect of viscosity of both continuous and to-be-dispersed phases on microchannel emulsification. At high ratios of the viscosities of the dispersed and continuous phases, the droplet size is not influenced, but at low viscosity ratios, the droplets become larger, and there is a ratio below which successful emulsification is not possible. This minimum viscosity ratio at which emulsification can still take place can be influenced by the design of the microchannel device; for example, a shorter terrace and longer channel lead to a lower critical ratio.

From CFD simulations, we found that the increased droplet size at low ratios is caused by the increased oil supply to the terrace due to a steeper pressure gradient in the continuous phase that surrounds the dispersed phase that is draining from the terrace. Surfactant dynamics are expected to have minor effects during droplet formation, although some secondary effects could play a role in the blow-up of the process, where depletion of available surfactant is expected to occur.

References

Anna SL, Bontoux N, Stone HA (2003) Formation of dispersions using "flow focusing" in microchannels. Appl Phys Lett 82:364–366

Garstecki P, Gitlin I, DiLuzio W, Whitesides GM, Kumacheva E, Stone HA (2004) Formation of monodisperse bubbles in a microfluidic flow-focusing device. Appl Phys Lett 85:2649–2651

Garstecki P, Fuerstman MJ, Stone HA, Whitesides GM (2006) Formation of droplets and bubbles in a microfluidic T-junction—scaling and mechanism of break-up. Lab Chip 6:437–446

Kawakatsu T, Kikuchi Y, Nakajima M (1997) Regular-sized cell creation in microchannel emulsification by visual microprocessing method. J Am Oil Chem Soc 74:317–321

Kobayashi I, Nakajima M, Chun K, Kikuchi Y, Fujita H (2002) Silicon array of elongated through-holes for monodisperse emulsion droplets. AIChE J 48:1639–1644

Kobayashi I, Mukataka S, Nakajima M (2004) CFD simulation and analysis of emulsion droplet formation from straight-through microchannels. Langmuir 20:9868–9877

Kobayashi I, Mukataka S, Nakajima M (2005) Novel asymmetric through-hole array microfabricated on a silicon plate for formulating monodisperse emulsions. Langmuir 21:7629–7632

Lucassen-Reynders EH, Kuijpers KA (1992) The role of interfacial properties in emulsification. Colloid Surf 65:175–184

Rayner M, Trägårdh G, Trägårdh C, Dejmek P (2004) Using the surface evolver to model droplet formation processes in membrane emulsification. J Colloid Interface Sci 279:175–185

Saito M, Yin L-J, Kobayashi I, Nakajima M (2005) Preparation characteristics of monodispersed oil-in-water emulsions with large particles stabilized by proteins in straight-through microchannel emulsification. Food Hydrocolloid 19:745–751

Sasaki M, Yasunaga T, Tatsumoto N (1977) Kinetic studies on double relaxation of surfactant solutions using a capillary wave method. Bull Chem Soc Jpn 50:3144–3148

Steegmans MLJ, Schroën K, Boom RM (2009) Characterization of emulsification at flat microchannel Y junctions. Langmuir 25:3396–3401

Sugiura S, Nakajima M, Seki M (2002) Effect of channel structure on microchannel emulsification. Langmuir 18:5708–5712

Sugiura S, Nakajima M, Oda T, Satake M, Seki M (2004) Effect of interfacial tension on the dynamic behavior of droplet formation during microchannel emulsification. J Colloid Interface Sci 269:178–185

van der Graaf S, Steegmans MLJ, van der Sman RGM, Schroën K, Boom RM (2005) Droplet formation in a T-shaped microchannel junction: a model system for membrane emulsification. Colloids Surf A 266:106–116

van Dijke KC, Schroën K, Boom RM (2008) Microchannel emulsification: from computational fluid dynamics to predictive analytical model. Langmuir 24:10107–10115

Vladisavljević GT, Kobayashi I, Nakajima M (2008) Generation of highly uniform droplets using asymmetric microchannels fabricated on a single crystal silicon plate: effect of emulsifier and oil types. Powder Technol 183:37–45

Vlahovska PM, Danov KD, Mehreteab A, Broze G (1997) Adsorption kinetics of ionic surfactants with detailed account for the electrostatic interactions. J Colloid Interface Sci 192:194–206

Xu Q, Nakajima M (2004) The generation of highly monodisperse droplets through the breakup of hydrodynamically focused microthread in a microfluidic device. Appl Phys Lett 85:3726–3728